Acta Scientiarum
http://periodicos.uem.br/ojs
ISSN on-line: 1807-8664
Doi: 10.4025/actascitechnol.v44i1.60577

Stress-strain analysis of the tow hook of a commercial truck by numerical simulations

Alexandre Assis Rezende Santos*, Leomar Santos Marques, Marcus Vinicius Ferreira de Moura and Ricardo Rodrigues Magalhães

Departamento de Automática, Universidade Federal de Lavras, Av. Doutor Sylvio Menicucci, 1001, 37200-000, Lavras, Minas Gerais, Brasil. *Author for correspondence. Email: alexrezendeufv@gmail.com

ABSTRACT. Numerical simulations have been widely used in the industry, although with some limitations. One of these limitations is the fact that the thermal effects derived from component manufacturing processes are normally disregarded in the analysis. Thus, the main goal of this study is to evaluate strains near the weld beads of a geometric model for a truck tow hook using numerical simulations by finite element method, considering thermal loads applied before the field loading. To validate the simulation results, an experiment was performed using a tow hook found in a commercial truck. Strain gauge rosettes were placed on the body base plate, and a load of 181.050 N was applied to the hook. This loading was the result of a commercial truck being pulled on level terrain, simulating a normal operation condition of the tow hook. The Von Mises stress found in simulations was approximately 302.23 MPa at the same position where the strain gauges were glued, when the load was applied. The difference between the simulated and experimental values of the equivalent specific strains in the area of the weld beads was 19.2%, and the difference between the permanent displacement values, resulting from plastic strain, in the X-direction was 0.1%. These results justify conducting new studies involving numerical simulations and considering thermal effects on static and dynamic loads in the automotive industry.

Keywords: Finite element method; plastic strain; strain gauge.

Received on August 17, 2021.
Accepted on October 21, 2021.

Introduction

Automotive components must be designed and manufactured properly and accurately to prevent possible failures under normal conditions of use. However, the guarantee that components will not fail in service is provided through strength and durability tests. These tests require time and money to obtain reliable results. To reduce product development costs and time, companies typically use resources derived from laboratory tests and numerical simulations. These simulations allow quickly changing the configurations of the numerical model and collecting data on the component. Nevertheless, in this type of analysis, the properties, manufacturing processes, and load conditions of the material should be studied. Numerical simulations provide faster results, but require calculating physical phenomena involved in the process, such as welding, at a high computational cost. To overcome this problem, simplified models are used, although without affecting the results. These simplified models are normally validated in experimental tests. In some cases, thermal analysis of a weld bead may determine the stress distribution in a part that is normally subjected to forces in the field. However, in most cases, the thermal input from the welding process of the part is disregarded, which may lead to inaccurate simulation results.

Some simulation studies about welding processes have been conducted (Chen & Soares, 2021; Rong, Xu, Huang, & Zhang, 2018; Venkatarao, 2021; Farias, Teixeira, & Vilarinho, 2021; Evdokimov et al., 2021) to identify stresses and strains along the weld beads. In these cases, models are commonly simplified and optimized, and the thermal load and residual stress involved in the welding process are disregarded. Doerk, Fricke, and Weissenborn (2003) compared different methods and procedures for calculating surface stresses in welded joints. Some methods are used for stress linearization through plate thickness, what followed the guidelines from the International Institute of Welding (IIW) to analyze certain types of weld beads.

Petracconi, Ferreira, and Palma (2010) conducted a study about the fatigue cracks initiation in the rear tow hook assembly of a passenger car. The authors compared experimental fatigue tests to numerical simulations disregarding welding effects. During the tests conducted by Petracconi et al. (2010), fatigue cracks were observed in the body base plate of the tow hook near the weld bead. The information needed to perform numerical analysis was retrieved from data collected using strain gauges. In this case, the strain gauges were glued close to the weld bead, disregarding the thermal load and the distortions in the tow hook structure resulting from the welding process of the part.

Magalhães, Vieira Junior, and Barra (2014) monitored stresses and strains with strain gauges during the welding process of steel plates. They performed numerical simulations to compare the results, although without applying the results to industrial processes or evaluating loads after the welding process through numerical simulations, requiring further research in this field.

Based on the above, the main goal of this study is to evaluate the stress-strain distribution near weld beads of a geometric model for a tow hook of a truck using numerical simulations, considering thermal loads before the field loads. The industry may benefit from this study because finite element analysis is a method widely used in the automotive industry that considers effects of thermal inputs from most industrial processes, such as welding and heat treatments, in addition to loads commonly used in numerical simulations, either static or dynamic.

Theoretical bases

Because the study of stresses and strains is not limited to the elastic regime, the standard equations of the principal stresses and strains cannot be used for this purpose. A stress-strain analysis out of the elastic zone requires defining hardening rules. The hardening rules determine the yield surface (flow rule), which determines the stress plane whereby stress flows, varying with the shape, size, and center. The most commonly used models for studying plasticity within hardening rules can be divided into the following categories: linear isotropic hardening and linear kinematic hardening.

The models differ regarding the shape, size, and position of the yield surface on the graph of the principal stresses. The conditions of the forces, physical properties, and amount of plastic strain applied to the sample may render the use of these models inappropriate.

For most metals and small strains, the linear kinematic hardening model (Bouhamed, Jrad, Said, Wali, & Dammak, 2019; Lee, Choi, Stoughton, & Yoon, 2019) is commonly applied. According to Lee et al. (2019) and Park, Stoughton, and Yoon (2019), the hardening rule predicts the anisotropic behavior and the Bauschinger effect of metals. The true stress-strain curve is necessary to study plasticity. As a linear model of kinematic hardening, the stress-strain curve is fitted to two curves (bilinear model), one representing the elastic regime and other the plastic regime. The slopes of the elastic and plastic curves are represented by Young's Modulus (E) and by the bulk modulus (K), both of which depend on the physical properties of the material. The modulus are given by Equation 1.

$$\frac{1}{K} = \frac{1}{E} + \frac{1}{HK} = \frac{1}{E} + \frac{1}{H} \qquad (1)$$

where E is Young's Modulus, K is the bulk modulus, and H is the plasticity modulus, which relates stress to true plastic strain.

The model whereby the curve is fitted to two curves is classified as an elastic-linear work-hardening model, and the bulk modulus is always smaller than Young's modulus. To calculate the bulk modulus, the true stress-strain curve must be first determined from the engineering stress-strain curve because using the true curve provides better information on forces acting along the plastic strain (Li, Yang, Siebert, Shi, & Yang, 2018; Pan & Chen, 2019; Zheng, Mashiwa, & Furushima, 2020). The equations that relate engineering to true stress and strain are defined by Equations 2 and 3.

$$\varepsilon_t = \ln(1+\varepsilon)\varepsilon_t = \ln(1+\varepsilon) \qquad (2)$$

$$\sigma_t = \sigma(1+\varepsilon)\sigma_t = \sigma(1+\varepsilon) \qquad (3)$$

Where ε is the specific strain of the material, ε_t is the true strain, σ is the engineering stress and σ_t is the true stress.

Once the equations that relate the engineering stress to the true stress and strain curves are defined (Equations 2 and 3), the bulk modulus can be calculated, and Equations 3 and 4 are valid only up to the ultimate tensile strength. For a finite element model of plastic strain, the analysis should also be considered non-linear. In this case, the equation 4 represents the solution of a non-linear model.

$$F_i = K_i u_i F_i = K_i u_i \tag{4}$$

Where F is the load applied to the nodes, K is the stiffness matrix of the element, and u represents the resulting nodal displacements. The index i represents the iteration number because the equation is solved "n" times until model convergence is reached; that is, in each iteration, new solutions and loads are presented because non-linear structures can be analyzed using a series of linear regressions, as shown in Figure 1. If the difference between the applied force and the internal force does not reach the minimum residual set, the model is not properly solved.

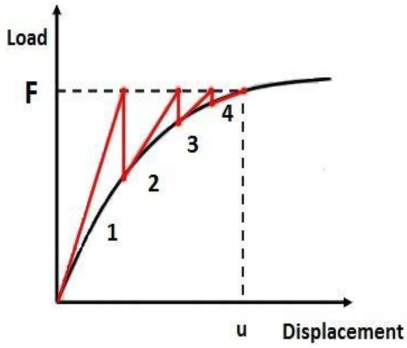

Figure 1. Newton-Raphson method for iterative linear regression analysis.

Material and methods

Simulation data

The geometric model for the tow hook was designed in two separate parts (body base plate and hitch pin, Figure 2). The hitch pin was disregarded in the simulations to reduce the computational cost. In this case, the load was distributed along the contact faces between the hitch pin and the body base plate to reproduce the hitch pin action in the system.

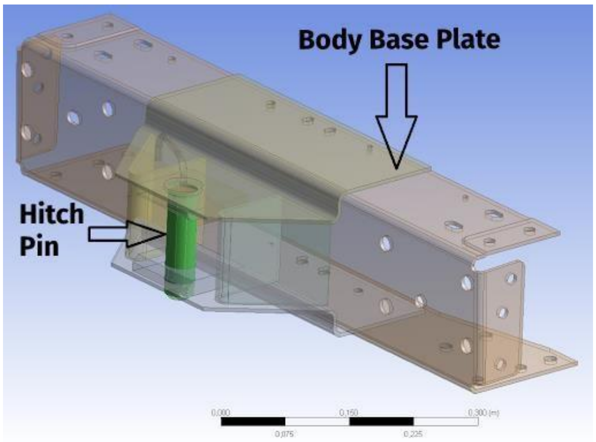

Figure 2. Computer-aided design (CAD) representation of the tow hook.

The pieces of the body base plate had a thickness of 4.75 millimeters, and the properties of the material were equivalent to structural steel, following the British standard BS EN 10002-1 (2001). The main mechanical properties of the material used in the body base plate are shown in Table 1.

The weld beads were simulated in the welded joints of the body base plate (Figure 3) using the gas metal arc welding (GMAW) process. The main physical properties used to simulate the welding process are described in Table 2.

Table 1. Mechanical properties of the study material.

Density (Kg m^{-3})	Young's modulus (GPa)	Poisson's ratio (mm mm^{-1})	Ultimate tensile strength (MPa)
7850	200	0.3	250

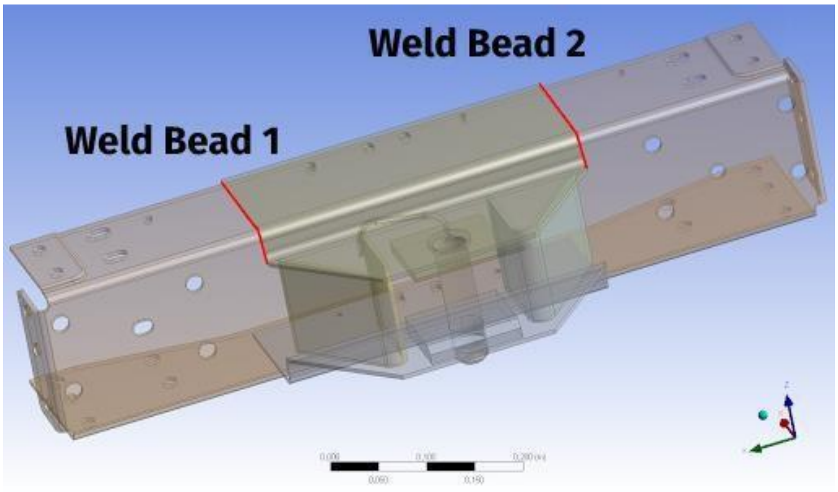

Figure 3. Representation of the weld beads used in the simulations.

Table 2. Properties of the weld beads.

Welding speed (mm s^{-1})	Heat flux (W $mm2^{-1}$)	Melting temperature (°C)	Welding time of each bead (s)
5	45	1130	27

The commercial software ANSYS, was used to perform the simulations in which the load was applied on the tow hook in several steps to reproduce the real load as well as possible. Because implementing oscillating and time-variant load point by point is time consuming, the initial (0 N) and final (181050 N) loads were entered into the software. Then, the software itself plotted consecutive points towards more reliably describing the real model and facilitating the configuration of the convergence parameters. The points closest to the original curve following line segments were selected, as shown in Figure 4.

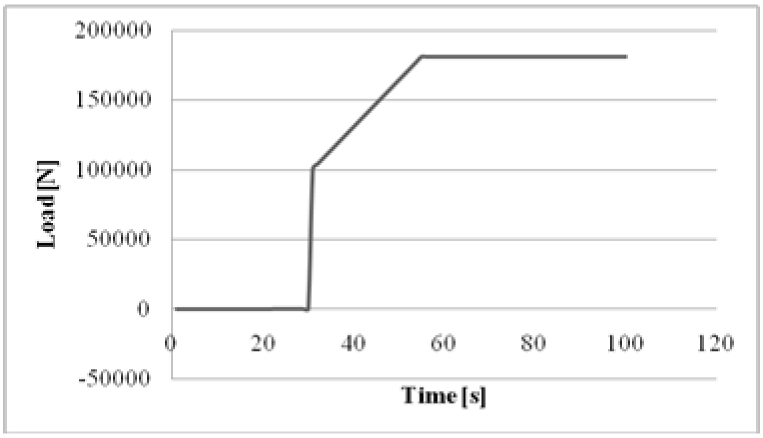

Figure 4. Load variation over time in the simulations.

To obtain the mesh used in the simulations, second-order tetrahedral and hexahedral elements were used. These elements support plasticity and hyper-elasticity studies. After mesh convergence, the body base plate model generated 310,291 nodes and 168,188 elements, as shown in Figure 5. The mesh convergence process was performed using commercial software, considering the same boundary conditions used in the simulations, although a static load without thermal effects was applied to reduce the computational cost of the mesh convergence process of the finite element model.

The study conducted by Derakhshan, Yazdian, Craft, Smith, and Kovacevic (2018) used some elements throughout the thickness of the study object. However, in the present study, only one element was considered when modeling the thickness, because a quadratic element does not require the use of another element (Maas, Ellis, Rawlins, & Weiss, 2016;Lee et al.(2020)). The study conducted by Doerk et al. (2003) used the thickness of a T-welded joint as the parameter to determine the size of the element. In the same study (Doerk et al., 2003), the length of the element was the same thickness of the plate, thus justifying the dimensions of the elements used to thicken the components of the body base plate, which was 4.75-mm thick.

In the simulations, the load applied to the faces where the hitch pin is coupled and the locking bolts of the body base plate on both side ends were analyzed, as shown in Figure 6.

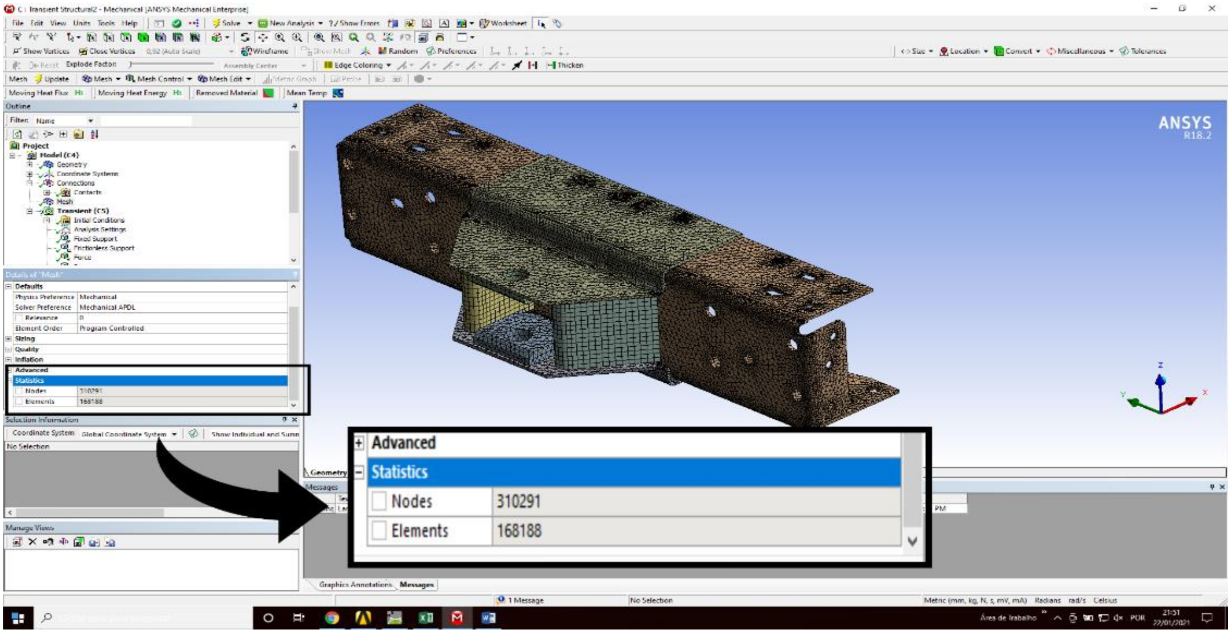

C : Transient Structural2 - Mechanical [ANSYS Mechanical Enterprise]

Details of "Mesh"

Defaults	
Physics Preference	Mechanical
Solver Preference	Mechanical APDL
☐ Relevance	0
Element Order	Program Controlled
Sizing	
Quality	
Inflation	
Advanced	
Statistics	
☐ Nodes	310291
☐ Elements	168188

Figure 5. Mesh of the body base plate used in the simulations.

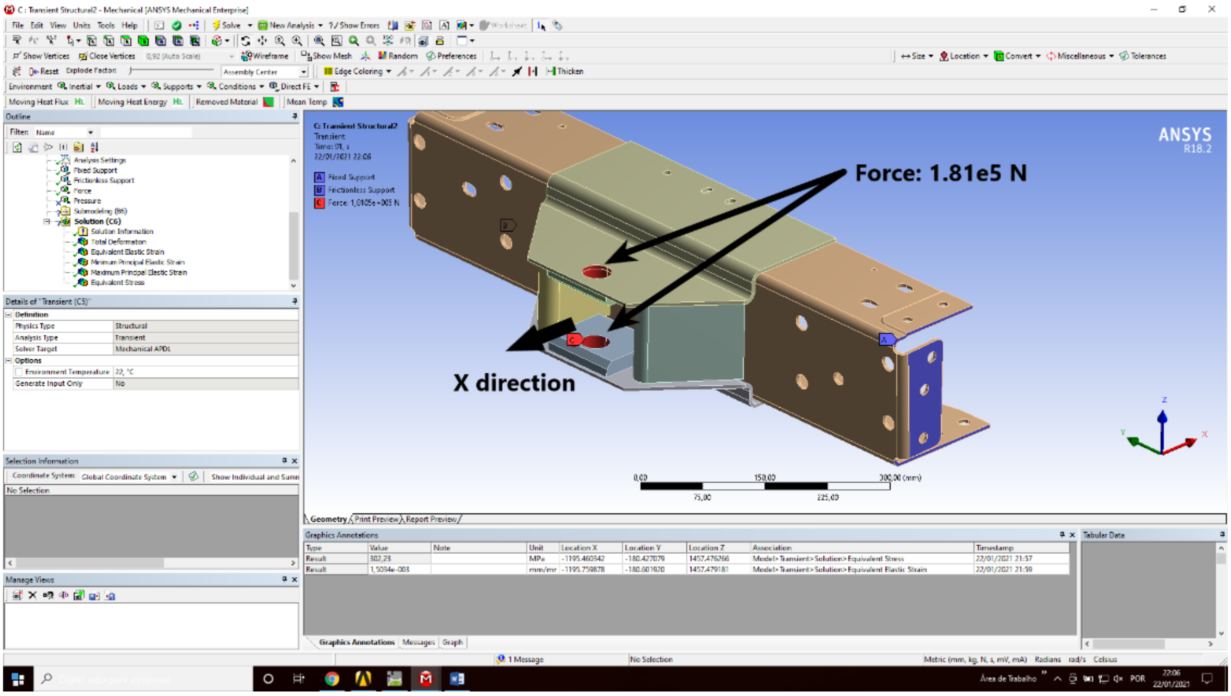

C : Transient Structural2 - Mechanical [ANSYS Mechanical Enterprise]

C: Transient Structural2
Transient
Time: 91, s
22/01/2021 22:06

A Fixed Support
B Frictionless Support
C Force: 1,8105e+005 N

Details of "Transient (C5)"

Definition	
Physics Type	Structural
Analysis Type	Transient
Solver Target	Mechanical APDL
Options	
☐ Environment Temperature	22, °C
Generate Input Only	No

Graphics Annotations

Type	Value	Note	Unit	Location X	Location Y	Location Z	Association	Timestamp
Result	302,23		MPa	-1195.460342	-180.427079	1457.476266	Model> Transient> Solution> Equivalent Stress	22/01/2021 21:57
Result	1,5034e-003		mm/mm	-1195.759878	-180.601920	1457.479181	Model> Transient> Solution> Equivalent Elastic Strain	22/01/2021 21:59

Figure 6. Boundary conditions for the numerical simulations.

Experimental data

In the experimental tests, the tow hook was coupled to a common truck with the wheels locked and in the gross vehicle weight (GVW) condition. Then, the tow hook was subjected to tensile testing through the motor action of another similar vehicle up to one of 181.050 N with the force acting only in the horizontal plane, as shown in Figure 7.

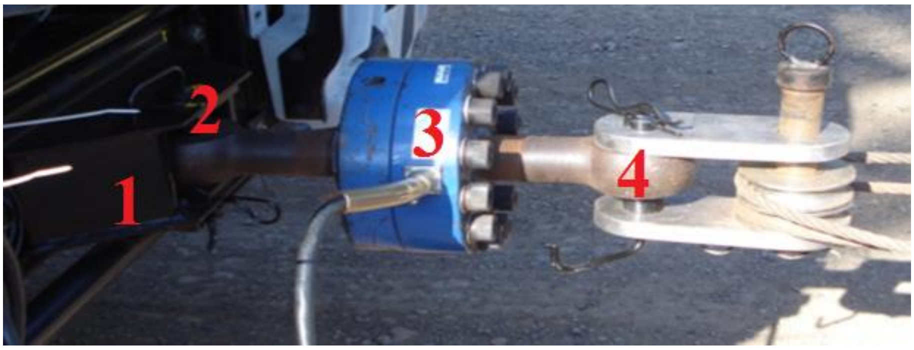

Figure 7. Load used in the experimental tests: (1) Body base plate; (2) Hitch pin; (3) Load cell; (4) Load.

An MGC data acquisition system (HDM) was used to collect data, a load cell with a capacity of 45 tons (Figure 7) was used to determine the applied load, and strain gauge rosettes were used to measure the strains. Two delta rosettes (three strain gauges arranged at 45°) were used to measure strain in both weld beads (right and left sides of the body base plate), as shown in Figure 8.

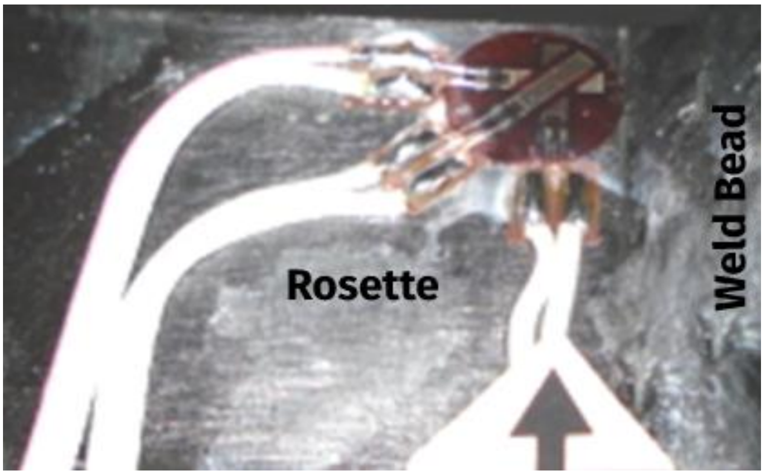

Figure 8. Rosette installation site on the right side of the body base plate.

Finally, the displacement along the X-axis was measured at a specific point of the body base plate using a dial indicator. This point (1) coincided with the location of the node chosen to monitor the displacements in the simulations (x = 1325, y = 182, z = 1420), as shown in Figure 9.

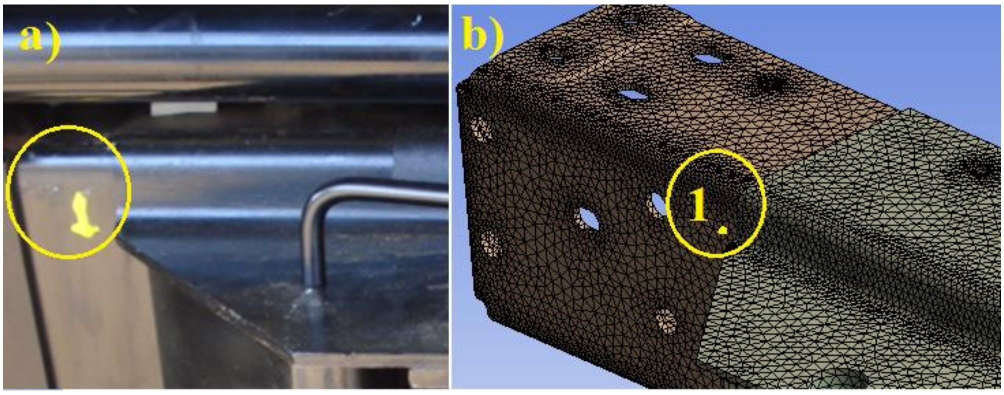

Figure 9. Measurement site of the real (a) and simulated (b) displacement along the X-direction.

Results and discussion

Simulation results

The graph resulting from the mesh convergence process is shown in Figure 10. The parameter used for convergence was the equivalent Von Mises stress, and the stability was 6.2%.

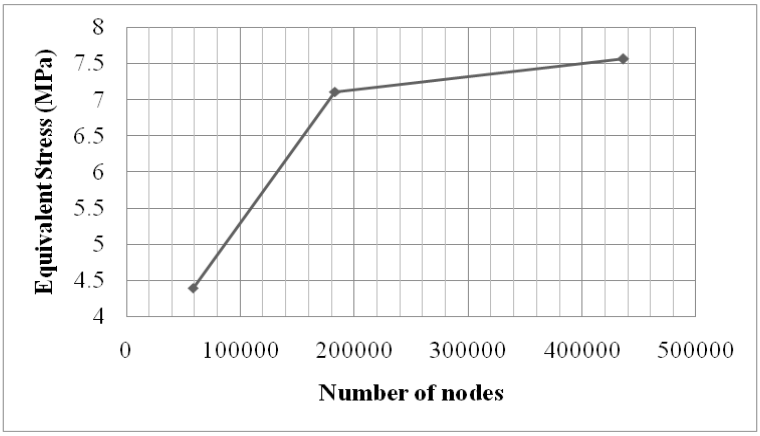

Figure 10. Mesh convergence of the model for the body base plate.

The results of temperatures derived from the heat input during welding are shown in Figures 11 and 12.

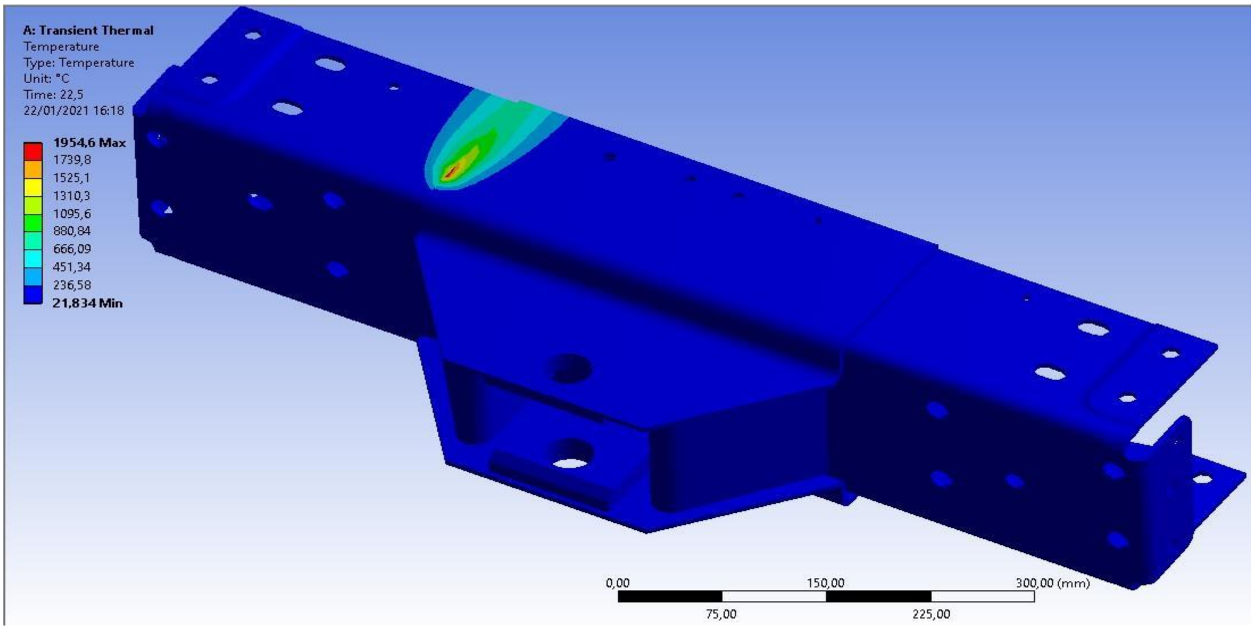

Figure 11. Simulated temperatures – Right side of the body base plate.

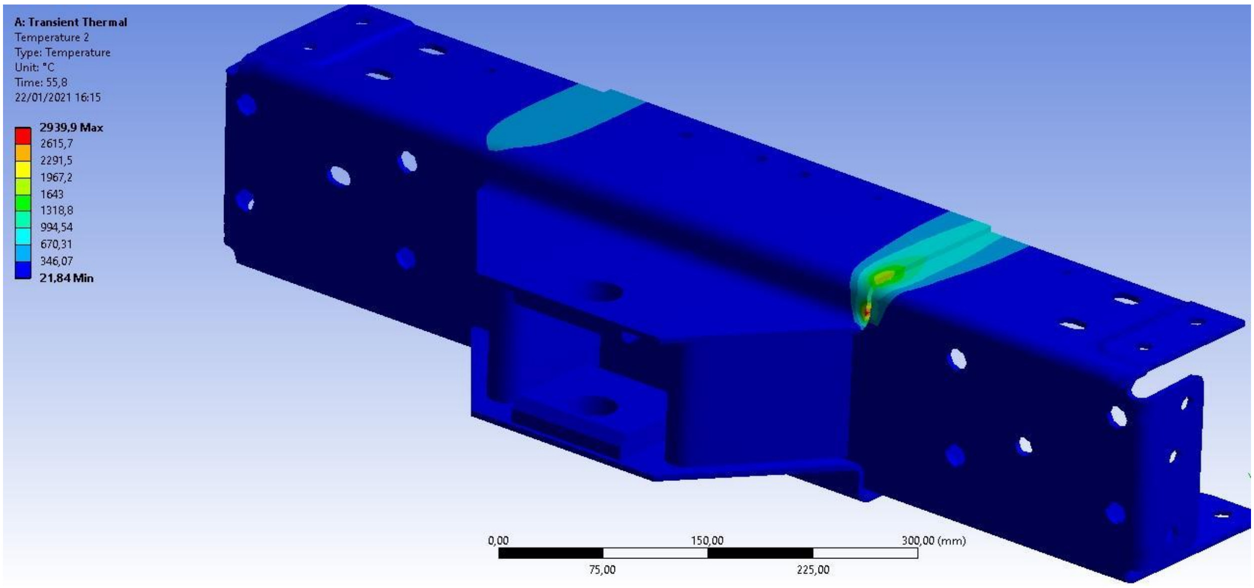

Figure 12. Simulated temperatures – Left side of the body base plate.

Figures 11 and 12 show the temperature effect on the representation of the weld beads and on the model of the real thermal load application to the component, which was not performed in the study by Doerk et al. (2003). The action of thermal load, combined with the subsequent application of the load of 181.050 N, originated Von Mises stresses, as shown in Figure 13.

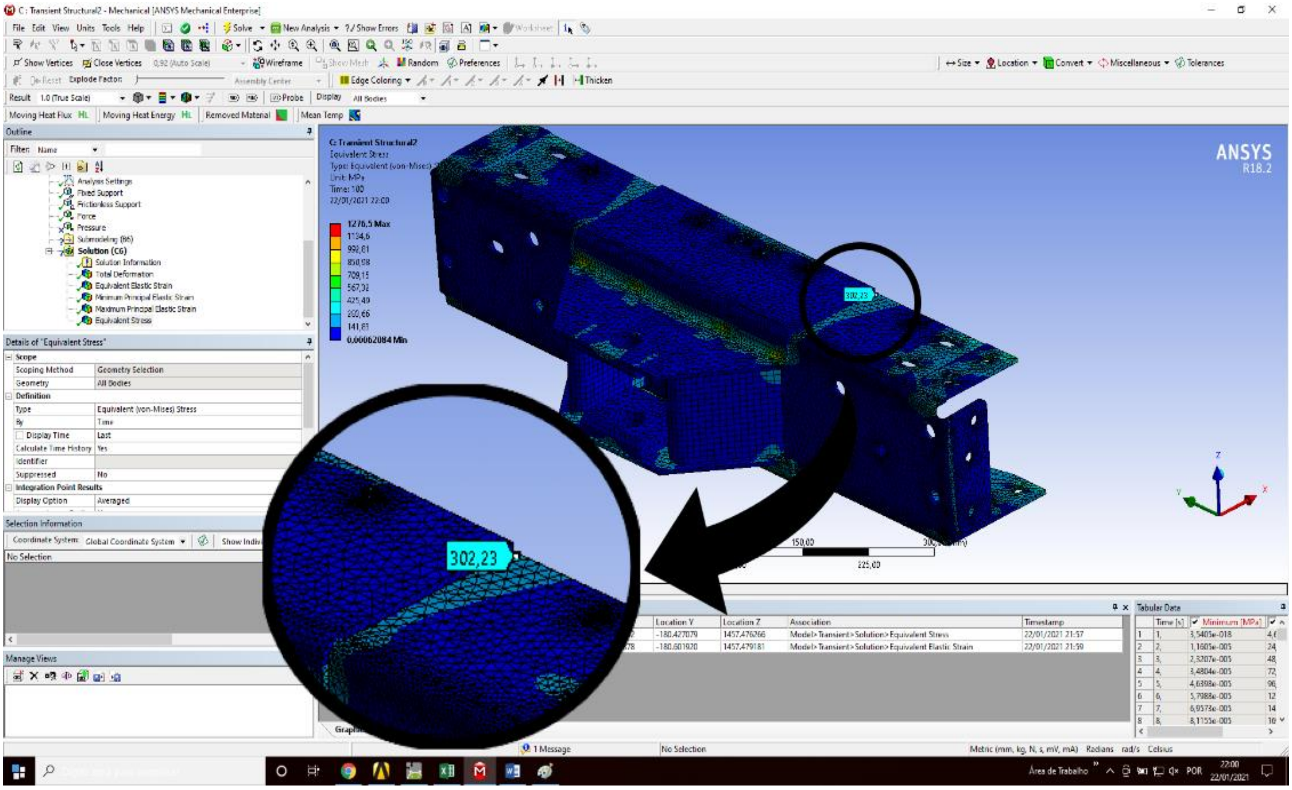
C: Transient Structural2 - Mechanical [ANSYS Mechanical Enterprise]

C: Transient Structural2
Equivalent Stress
Type: Equivalent (von-Mises) Stress
Unit: MPa
Time: 100
22/01/2021 22:00

1276,5 Max
1134,6
992,81
850,98
709,15
567,32
425,49
283,66
141,83
0,00062084 Min

Details of "Equivalent Stress"

Scope	
Scoping Method	Geometry Selection
Geometry	All Bodies
Definition	
Type	Equivalent (von-Mises) Stress
By	Time
☐ Display Time	Last
Calculate Time History	Yes
Identifier	
Suppressed	No
Integration Point Results	
Display Option	Averaged

Location Y	Location Z	Association	Timestamp
-180.427079	1457.476266	Model> Transient> Solution> Equivalent Stress	22/01/2021 21:57
-180.601920	1457.479181	Model> Transient> Solution> Equivalent Elastic Strain	22/01/2021 21:59

Tabular Data

	Time [s]	✓ Minimum [MPa]
1	1,	3,5405e-018
2	2,	1,1605e-005
3	3,	2,3207e-005
4	4,	3,4804e-005
5	5,	4,6398e-005
6	6,	5,7988e-005
7	7,	6,9573e-005
8	8,	8,1155e-005

No Selection

Metric (mm, kg, N, s, mV, mA) Radians rad/s Celsius

Figure 13. Simulated Von Mises stresses in the body base plate.

Figure 13 shows that, in the area close to the weld bead, the Von Mises stress values were approximately 302 MPa. This value is higher than the ultimate tensile strength of the material used in the simulations (250 MPa, Table 1), which suggests plastic strain of the material.

In some studies as Jang, Chang, and Lee (2007), it was analyzed residual stresses on 10-mm-thick T-welded tubular joint. In some points, around the weld bead, these residual stresses reached maximum values of 400 MPa approximately.

The residual stresses generated in Jang et al.(2007) are caused by thermal shrinkage, because during the solidification and cooling of the weld beads, its volume is reduced, pulling the substrate around the welding. These residual stresses were significant and might amplify stresses produced when the component is used, and thus reach even higher stress levels through this addition.

Furthermore, the thermal source applied to build the part can weaken the material around the weld through the heat-affected zone (HAZ). The simulations of displacement of the material along the X-direction, resulting from the welding process and subsequent load, showed maximum values of 1.3 mm in the central area of the body base plate and 0.90563 mm close to the area of the weld bead, Figure 14.

An aspect that should be considered in the simulations, but it was ignored in this study, was to account for the mechanical properties of the weld bead material. Generally, the mechanical strength and hardness of the material are higher than those of the base material. As a result, the stiffness of the study material is higher in the weld bead, which may alter the stress results around the weld bead, thus affecting the values found in the simulations. In terms of the specific strain, the values found in the simulations are shown in Figure 15.

In figure, 15 are shown that the stress derived from the welding process and a subsequent load of 181.050 N on the hitch pin of the tow hook ranged from 5.2e^{-3} to 1.245e^{-2}, considering areas close to the beginning and end of the weld bead on the left side of the body base plate.

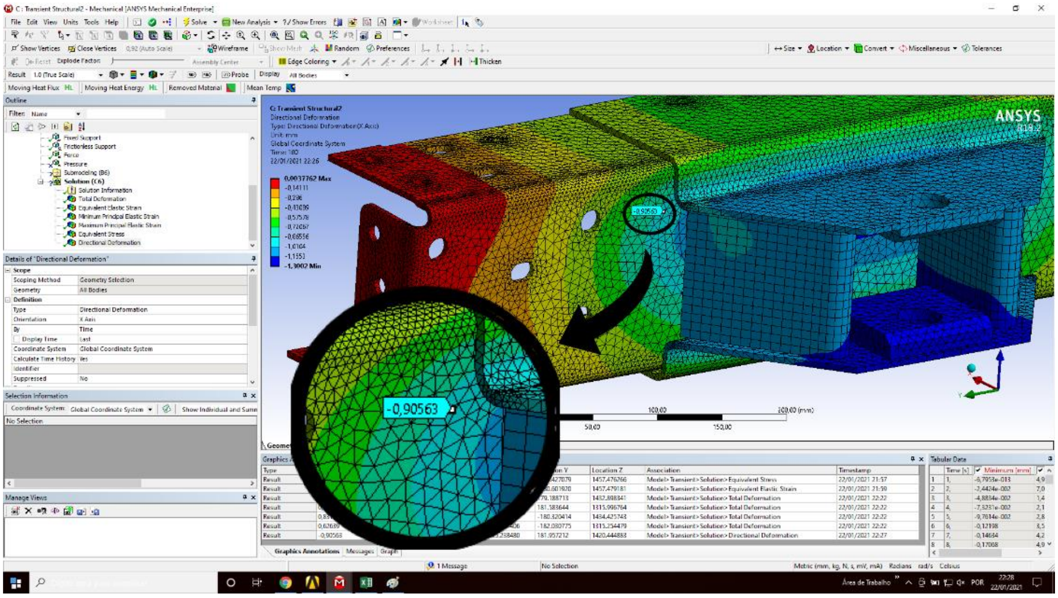

Details of "Directional Deformation"

Scope	
Scoping Method	Geometry Selection
Geometry	All Bodies
Definition	
Type	Directional Deformation
Orientation	X Axis
By	Time
☐ Display Time	Last
Coordinate System	Global Coordinate System
Calculate Time History	Yes
Identifier	
Suppressed	No

Selection Information

Coordinate System: Global Coordinate System

No Selection

Location Z	Association	Timestamp
1457.476266	Model> Transient> Solution> Equivalent Stress	22/01/2021 21:57
1457.479181	Model> Transient> Solution> Equivalent Elastic Strain	22/01/2021 21:59
1432.898341	Model> Transient> Solution> Total Deformation	22/01/2021 22:22
1315.996764	Model> Transient> Solution> Total Deformation	22/01/2021 22:22
1434.425743	Model> Transient> Solution> Total Deformation	22/01/2021 22:22
1315.254479	Model> Transient> Solution> Total Deformation	22/01/2021 22:22
1420.444883	Model> Transient> Solution> Directional Deformation	22/01/2021 22:27

Tabular Data

	Time [s]	Minimum [mm]
1	1,	-6,7953e-013
2	2,	-2,4424e-002
3	3,	-4,8834e-002
4	4,	-7,3231e-002
5	5,	-9,7614e-002
6	6,	-0,12198
7	7,	-0,14634
8	8,	-0,17068

No Selection

Metric (mm, kg, N, s, mV, mA) Radians rad/s Celsius

Figure 14. Displacements simulated in the body base plate along the X-direction.

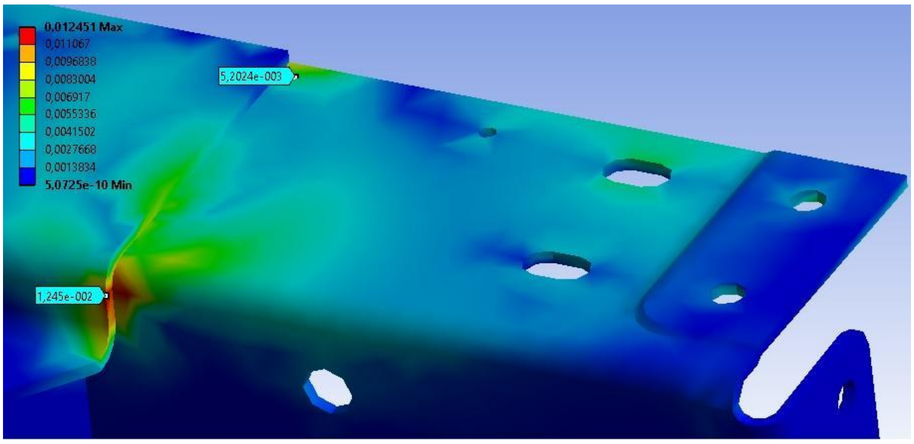

Figure 15. Simulated equivalent specific strains.

Experimental results

To validate the simulations, a load of 181.050 N was applied over time on the tow hook, as shown in Figure 16. It was considered a quasi-static system in the analysis, because the forces were applied gradually to prevent overstressing.

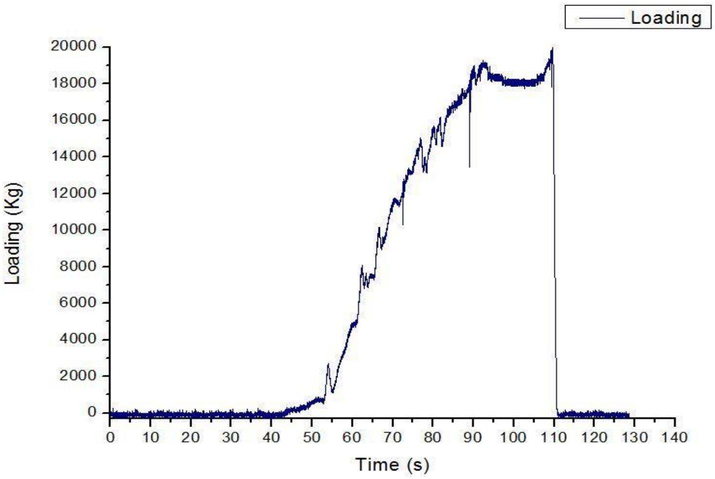

Figure 16. Tensile force applied to the tow hook.

The strains measured using each strain gauge rosette (right and left sides of the body base plate) are shown in Figures 17 and 18.

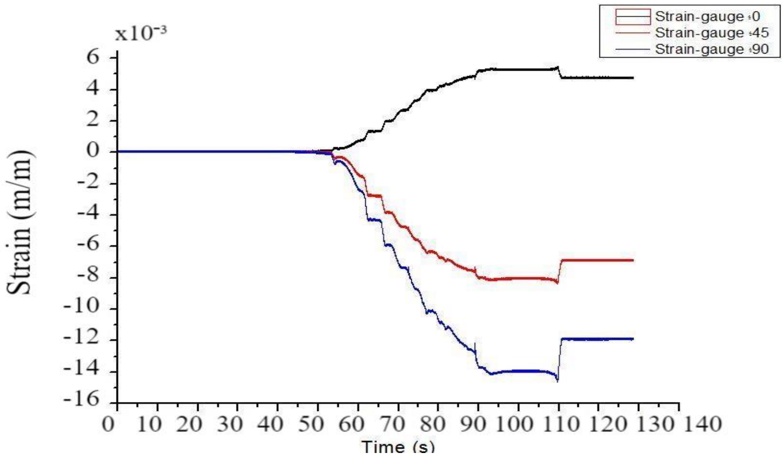

Figure 17. Strains occurred in the strain gauge rosettes on the right side of the tow hook.

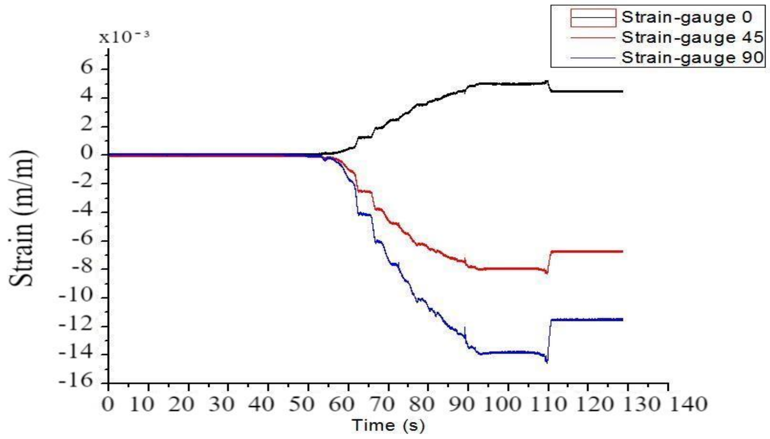

Figure 18. Strains occurred in the strain gauge rosettes on the left side of the tow hook.

The analysis of the specific strain results in the graphs of Figures 17 and 18 shows that the strain gauge curves corresponding to the left and right sides had similar values. Therefore, the strain values can be analyzed independently of the body base plate.

The strain values of each strain gauge, corresponding to a time of 105 s within the constant load zone (181.050 N), were determined from data collected in the graphs of Figures 17 and 18. The values are shown in Table 3.

Table 3. Strain values at 105 s.

	Strain gauge 0° (μm m^{-1})	Strain gauge 45° (μm m^{-1})	Strain gauge 90° (μm m^{-1})
Right-side rosette	5,296.64	-8,006.03	-13,919.20
Left-side rosette	5,023.74	-7,904.60	-13,780.15

Finally, the history of equivalent specific strains measured using strain gauges was raised, as shown in Figure 19.

Figure 19 shows the occurrence of an analyzed plastic strain of the material at the position where the rosette was glued, as confirmed by the incomplete recovery of the structure when ceasing the loading on the tow hook (from a time of 110 s). The permanent displacement measured along the X-axis at a specific point of the body base plate (Figure 9) was 0.9 mm.

Comparison between simulated and experimental results

The simulated and experimental properties results were compared considering a time of 100 s when the load stabilized at 181.050 N and are shown in Table4.

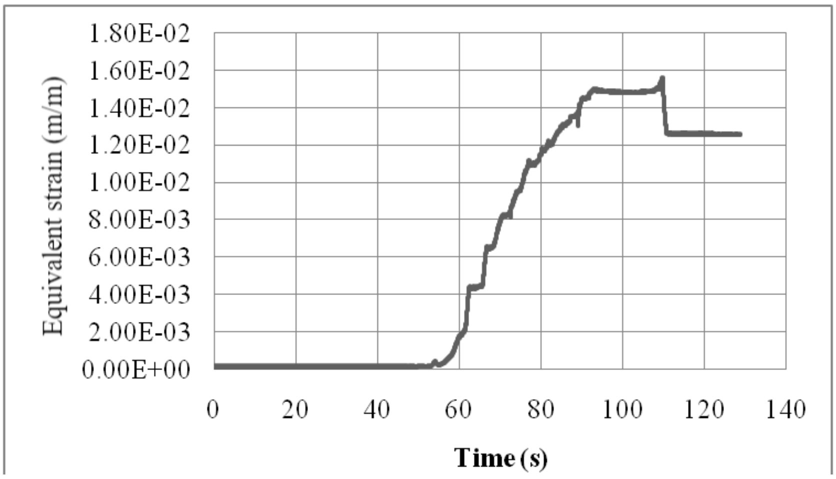

Figure 19. Equivalent specific strains– Right side of the body base plate.

Table 4. Comparison between the results from experimental tests and simulations.

Properties	Equivalent specific strain (mm mm^{-1})	Permanent displacement (mm)
Experimental tests	1.49 e-2	0.90
Simulations	1.25 e-2	0.91
Difference	19.2%	0.1%

Table 4 shows a difference of approximately 19% between the simulated and real values of the maximum equivalent specific strain. The reason for this difference between experimental and simulated results may be due to inefficient modeling of thermal shrinkage for complex structures and the material of the weld not being considered in the simulation. However, this difference can be considered acceptable, since Magalhães et al. (2014) found a difference of 35% between simulated and real stress values. Although these values do not overlap in the body base plate, they are located in areas close to the weld bead. When considering the same position, the difference between the values is significantly higher. However, the difference between the simulated and real permanent displacement values is only 0.1%, which indicates future opportunities for applying numerical simulations considering the thermal effects of industrial processes.

Conclusion

. The Von Mises stresses found in simulations were approximately 302.23 MPa, occurring plastic deformation of body base plate (250 MPa), and this effect was observed in the experiment.

. The difference between the simulated and real values of equivalent specific strain at the weld beads was 19.2%. Despite being higher, the differences found in the literature when welding thermal effects are considered in simulations is lower.

. In terms of permanent displacement along the X-direction, the difference was only 0.1%, which justifies conducting further academic and industrial research through numerical simulations of thermal effects on static and dynamic loads.

References

Bouhamed, A., Jrad, H., Said, L. B., Wali, M., & Dammak, F. (2019). A non-associated anisotropic plasticity model with mixed isotropic–kinematic hardening for finite element simulation of incremental sheet metal forming process. *The International Journal of Advanced Manufacturing Technology, 100*(1), 929–940. DOI: http://doi.org/10.1007/s00170-018-2782-3

Chen, B.-Q., & Soares, C. G. (2021). Experimental and numerical investigation on welding simulation of long stiffened steel plate specimen. *Marine Structures, 75*, 102824. DOI: http://doi.org/10.1016/j.marstruc.2020.102824

Derakhshan, E. D., Yazdian, N., Craft, B., Smith, S., & Kovacevic, R. (2018). Numerical simulation and experimental validation of residual stress and welding distortion induced by laser-based welding processes of thin structural steel plates in butt joint configuration. *Optics & Laser Technology, 104*, 170–182. DOI: http://doi.org/10.1016/j.optlastec.2018.02.026

Doerk, O., Fricke, W., & Weissenborn, C. (2003). Comparison of different calculation methods for structural stresses at welded joints. *International Journal of Fatigue, 25*(5), 359–369. DOI: http://doi.org/10.1016/S0142-1123(02)00167-6

Evdokimov, A., Doynov, N., Ossenbrink, R., Obrosov, A., Weiß, S., & Michailov, V. (2021). Thermomechanical laser welding simulation of dissimilar steel-aluminum overlap joints. *International Journal of Mechanical Sciences, 190*, 106019. DOI: http://doi.org/10.1016/j.ijmecsci.2020.106019

Farias, R. M., Teixeira, P. R. F., & Vilarinho, L. O. (2021). An efficient computational approach for heat source optimization in numerical simulations of arc welding processes. *Journal of Constructional Steel Research, 176*, 106382. DOI: http://doi.org/10.1016/j.jcsr.2020.106382

Jang, G. C., Chang, K. H., & Lee, C. H. (2007). Characteristics of the residual stress distribution in welded tubular T-joints. *Journal of Mechanical Science and Technology, 21*(10), 1714. DOI: http://doi.org/10.1007/BF03177399

Lee, E.-H., Choi, H., Stoughton, T. B., & Yoon, J. W. (2019). Combined anisotropic and distortion hardening to describe directional response with Bauschinger effect. *International Journal of Plasticity, 122*, 73–88. DOI: http://doi.org/10.1016/j.ijplas.2019.07.007

Lee, J., Bong, H. J., Kim, D., Lee, Y.-S., Choi, Y., & Lee, M.-G. (2020). Mechanical Properties and Formability of Heat-Treated 7000-Series High-Strength Aluminum Alloy: Experiments and Finite Element Modeling. *Metals and Materials International*, *26*(5), 682–694. https://doi.org/10.1007/s12540-019-00353-9

Li, J., Yang, G., Siebert, T., Shi, M. F., & Yang, L. (2018). A method of the direct measurement of the true stress–strain curve over a large strain range using multi-camera digital image correlation. *Optics and Lasers in Engineering, 107*, 194–201. DOI: http://doi.org/10.1016/j.optlaseng.2018.03.029

Maas, S. A., Ellis, B. J., Rawlins, D. S., & Weiss, J. A. (2016). Finite element simulation of articular contact mechanics with quadratic tetrahedral elements. *Journal of Biomechanics, 49*(5), 659-667. DOI: http://doi.org/10.1016/j.jbiomech.2016.01.024

Magalhães, R. R., Vieira Junior, A. B., & Barra, S. R. (2014). The use of conventional strain gauges evaluation for measurements of residual stresses in welded joints. *Journal of the Brazilian Society of Mechanical Sciences and Engineering, 36*(1), 173–180. DOI: http://doi.org/10.1007/s40430-013-0082-2

Pan, B., & Chen, B. (2019). A novel mirror-assisted multi-view digital image correlation for dual-surface shape and deformation measurements of sheet samples. *Optics and Lasers in Engineering, 121*, 512–520. DOI: http://doi.org/10.1016/j.optlaseng.2019.05.016

Park, N., Stoughton, T. B., & Yoon, J. W. (2019). A criterion for general description of anisotropic hardening considering strength differential effect with non-associated flow rule. *International Journal of Plasticity, 121*, 76–100. DOI: http://doi.org/10.1016/j.ijplas.2019.04.015

Petracconi, C. L., Ferreira, S. E., & Palma, E. S. (2010). Fatigue life simulation of a rear tow hook assembly of a passenger car. *Engineering Failure Analysis, 17*(2), 455–463. DOI: http://doi.org/10.1016/j.engfailanal.2009.09.002

Rong, Y., Xu, J., Huang, Y., & Zhang, G. (2018). Review on finite element analysis of welding deformation and residual stress. *Science and Technology of Welding and Joining, 23*(3), 198–208. DOI: http://doi.org/10.1080/13621718.2017.1361673

Venkatarao, K. (2021). The use of teaching-learning based optimization technique for optimizing weld bead geometry as well as power consumption in additive manufacturing. *Journal of Cleaner Production, 279*, 123891. DOI: http://doi.org/10.1016/j.jclepro.2020.123891

Zheng, Q., Mashiwa, N., & Furushima, T. (2020). Evaluation of large plastic deformation for metals by a non-contacting technique using digital image correlation with laser speckles. *Materials & Design, 191*, 108626. DOI: http://doi.org/10.1016/j.matdes.2020.108626